



# Weld thermal simulation of API 5CT L80 grade steel

Vinothkumar Palanisamy<sup>1</sup> · Jan Ketil Solberg<sup>1</sup> · Bjarne Salberg<sup>2</sup> · Per Thomas Moe<sup>2,3</sup>

Received: 6 January 2021 / Accepted: 25 May 2021 / Published online: 6 June 2021  
© The Author(s) 2021

## Abstract

The microstructure and mechanical properties of an API 5CT L80 casing grade steel (0.24C 0.4Si 1.4Mn CrNiCu) have been studied after performing weld thermal simulations (with and without subsequent tempering) applying a thermal cycle weld simulator. Specimens were subjected to three different peak temperatures (1300 °C, 1150 °C, 950 °C) and five different cooling rates (1 °C/s, 3 °C/s, 5 °C/s, 10 °C/s, 60 °C/s) through the austenite transformation temperature range. Based on the microstructure, hardness values, and toughness properties of the simulated specimens, thermal cycles were selected and recommended for welding of L80 components by the SAG-FW (shielded active gas forge welding) method.

**Keywords** Forge welding · L80 casing grade steel · Thermal simulation · Shielded active gas forge welding

## 1 Introduction

Welding of high carbon equivalent (i.e. >0.53) steels has always been a challenge in the engineering industry. The stringent requirements for oil and gas applications demand better processing methods and excellent weld quality for safety and environment care. After an oil/gas well has been drilled, a pipe (casing) is inserted into the borehole to support its walls from caving. Steel tubes for casing applications must have high

tensile strength, internal pressure strength, and collapsing strength. Commonly used casing grade steels satisfying the API 5CT specifications are J55, K55, H40, N80-1, N80Q, and P110. Due to the well conditions and sour environments, the corrosion resistance of the alloys has also to be considered. Grades of corrosion-resistant API 5CT steels are L80, C90, M65, C95, and T95. Due to their high carbon contents (0.2–0.5 wt% C), these steels have poor weldability by fusion. Threaded connections are therefore commonly used, but these may leak if they are deformed when they are expanded downhole, which is an important reason for selecting forge welded connectors.

The shielded active gas forge welding (SAG-FW) method has been developed to weld high carbon steels in a rapid and efficient way. This method has been tested on several steel grades like AISI 316, API 5L X65, API 5CT K55, API 5CT J55, and API 5CT L80 using a laboratory-developed small-scale forge welding machine [1, 2]. The welding temperature and cooling rate are two of the most important parameters that determine the microstructure and mechanical properties of a weld. Therefore, as an initial screening stage in a successive development of welding parameters for the SAG-FW process, one may leave out the forging step and only study the effect of the welding temperature and cooling rate on the weld properties. This simplified test procedure can be carried out by applying a SMITWELD thermal cycle simulator® (TCS) with a simple specimen geometry, drastically reducing the machining costs of full SAG-FW simulations. Several authors have done thermal simulations of carbon steels using either a SMITWELD simulator [e.g. 3, 4], or a Gleeble1500 simulator

Recommended for publication by Commission IX - Behaviour of Metals Subjected to Welding

✉ Jan Ketil Solberg  
jan.ketil.solberg@ntnu.no

Vinothkumar Palanisamy  
vinothvp@gmail.com

Bjarne Salberg  
bjame.salberg@gmail.com

Per Thomas Moe  
Per.T.Moe@usn.no

<sup>1</sup> Department of Materials Science and Engineering, Norwegian University of Science and Technology, Alfred Getz vei 2, N-7034 Trondheim, Norway

<sup>2</sup> AMR Engineering AS, Rosenkrantzgata 61B, N-3018 Drammen, Norway

<sup>3</sup> Department of Science and Industry Systems, University of South-Eastern Norway, Hasbergvei 36, Krona, 3616 Kongsberg, Norway

[5–7]. A comparison of results obtained by TCS with real welded joints by arc welding is presented in [3]. Of course, unlike the case of arc welding, microstructures and mechanical properties obtained by TCS do not directly correspond to those obtained after forge welding since the high temperature plastic deformation introduced during the latter process results in recrystallization and grain refinement of the austenite. This will in turn lead to more refined and probably tougher final microstructures. Finer austenite grains will also have an influence on the steel hardenability and the final hardness, the effect on hardness being dependent on the cooling rate. However, TCS experiments are still a useful tool in the development of thermal parameters for forge welding. Such experiments generate the same variety of microstructures and properties that would be present in the weld zone after forge welding, the main differences being caused by the larger prior austenite grain size during TCS. The forging stage during forge welding has much of the same effect on the final microstructure as a reduction in the peak temperature during TCS. Moreover, TCS parameters that give acceptable toughness values should in most cases give acceptable toughness properties after forge welding since the forging stage results in refined microstructures. Fulfilment of the hardness requirements on the weld needs, however, closer consideration.

In this investigation, a casing grade API 5CT L80 steel has been subjected to different thermal cycles in a thermal cycle simulator (TCS). Based on the observed microstructures, hardness values, and Charpy-V impact strength values, a series of thermal cycles have been suggested for welding by the small-scale forge welding (SSFW) method.

## 2 Experimental details

The tube steel subjected to experiments in this study was an API 5CT L80 (min. yield strength 80 ksi/550 MPa) casing

grade steel containing 0.24% C produced by OAO Volzhsky Pipe Plant, Volgograd, Russia. The actual chemical composition and mechanical properties of L80 are given in Table 1, which also includes three transformation temperatures that were calculated from the equations given in the table. A hot rolled L80 pipe was received as a large diameter pipe with nominal wall thickness 11 mm and outer diameter 244 mm with a microstructure of tempered martensite (Fig. 1). Thermal simulation samples with dimensions  $100 \times 10 \times 5 \text{ mm}^3$  were machined from the pipe wall with the 100 mm dimension along the longitudinal direction of the pipe and the 10 mm dimension along the radial direction of the pipe. The samples were machined with a ground surface finish. All thermal weld simulations were carried out using a SMITWELD Thermal Cycle Simulator® (TCS) 1405. The SMITWELD simulator is standard equipment, and the experimental setup is not included here. A detailed sketch is, however, presented in Ref. [4]. The thermal simulation specimens are clamped between two water-cooled jaws, and the specimen cross section required for heating is  $11 \times 11 \text{ mm}^2$  to have electrical contact with the jaws. Copper spacers were used in the case of the  $10 \times 5 \text{ mm}^2$  steel specimens to obtain electrical contact between the jaws and the specimens. A K-type Chromel-Alumel thermocouple was spot welded on to the specimen surface, halfway between the jaws, to continuously record the temperature and store it in the system software. The jaws were cooled by water circulation. The distance between the jaws influences the maximum and minimum limits of heating rate and cooling rate. Smaller distance between the jaws gives a higher cooling rate. The distance between the jaws used to achieve  $10 \text{ }^\circ\text{C/s}$  and  $60 \text{ }^\circ\text{C/s}$  cooling rates was 10.5 mm. A distance of 14.5 mm was used for  $1 \text{ }^\circ\text{C/s}$ ,  $3 \text{ }^\circ\text{C/s}$ , and  $5 \text{ }^\circ\text{C/s}$  cooling rates. A dilatometer was positioned across the large thickness direction to record maximum dimension changes.

In this study, three different welding (or peak) temperatures,  $1300 \text{ }^\circ\text{C}$ ,  $1150 \text{ }^\circ\text{C}$ , and  $950 \text{ }^\circ\text{C}$ , were chosen based on relevant temperatures for shielded active gas forge welding. A

**Table 1** Material chemistry, mechanical properties, and calculated transformation temperatures of as received steel

Element	C	Si	Mn	P	S	Cr	Ni	Cu	Al	Mo	V	Fe
Wt%	0.24	0.4	1.37	0.01	0.005	0.14	0.14	0.2	0.01	0.02	0.005	Bal.
Material properties												
Toughness (J) $0 \text{ }^\circ\text{C}$									143			
Hardness (HV10)									232			
$A_{c3}$ temperature ( $^\circ\text{C}$ )									827			
$B_s$ ( $^\circ\text{C}$ )									625			
$M_s$ ( $^\circ\text{C}$ )									392			

$$A_{c3}(\text{ }^\circ\text{C}) = 910 - 203(\text{wt}\% \text{C})^{1/2} - 15.2(\text{wt}\% \text{Ni}) + 44.7(\text{wt}\% \text{Si}) + 104(\text{wt}\% \text{V}) + 31.5(\text{wt}\% \text{Mo}) + 13.1(\text{wt}\% \text{W}) \quad [8]$$

$$B_s(\text{ }^\circ\text{C}) = 830 - 270\text{C} - 90\text{Mn} - 37\text{Ni} - 70\text{Cr} - 83\text{Mo} \quad [9]$$

$$M_s(\text{ }^\circ\text{C}) = 539 - 423(\text{wt}\% \text{C}) - 30.4(\text{wt}\% \text{Mn}) - 17.7(\text{wt}\% \text{Ni}) - 12.1(\text{wt}\% \text{Cr}) - 7.5(\text{wt}\% \text{Mo}) \quad [8]$$

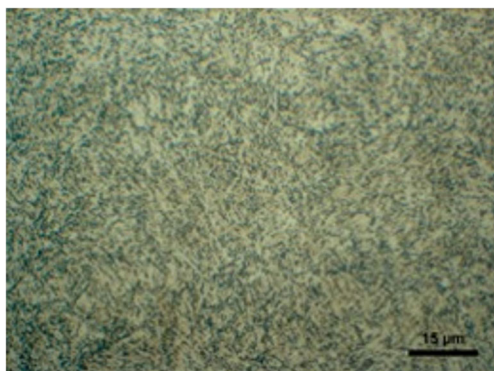
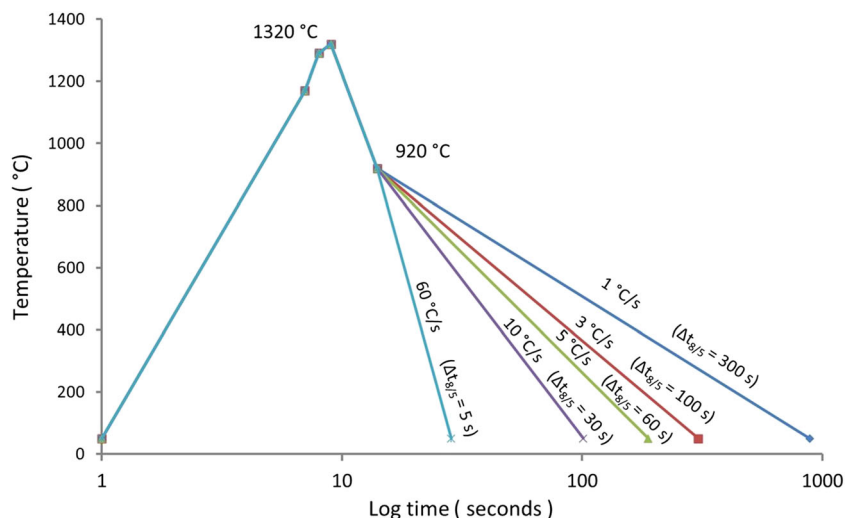


**Fig. 1** The tempered martensitic microstructure of the as received steel pipe

constant heating time of 8 s was used in all cases to achieve the peak temperature. The heating rate was gradually reduced when the temperature approached the peak temperature. Immediately after reaching the peak temperature, all specimens were cooled as quickly as possible (60 °C/s) down to 920 °C. From 920 °C, five different controlled cooling (CC) rates, i.e. 1 °C/s, 3 °C/s, 5 °C/s, 10 °C/s, and 60 °C/s (the highest obtainable), were chosen for further cooling down to room temperature (see Fig. 2). The cooling time between 800 and 500 °C,  $\Delta t_{8/5}$ , corresponding to each individual cooling rate has been given in the figure. The simulated temperature cycles correspond closely to those of the actual SAG-FW process in which efforts have been made to implement various ways of controlling the cooling rate after welding. A cooling rate of 60 °C/s corresponds to quenching the weld by water. A cooling rate of 1 °C/s corresponds to very slow cooling with some heat provided by an induction heating coil positioned close to the weld. Intermediate cooling rates can be obtained from natural cooling due to heat conduction as well as convection and radiation to the surrounding air. The natural cooling rate depends on the temperature distribution after forging. This distribution will always be very non-uniform

**Fig. 2** Input parameters for controlled cooling cycles for the 1300°C peak temperature



to allow for localized deformation. The rapid cooling down to 920 °C is also characteristic for the SAG-FW process because a high temperature gradient causes the temperature to drop very fast in the beginning before a coil can be introduced for slower cooling. This initial temperature reduction is beneficial for limiting austenite grain growth.

Two specimens A and B were produced for each controlled cooling rate condition, and specimen B of each couple was, after the temperature cycle, tempered in the TCS machine at 680 °C for 1 s. The heating time to 680 °C was 4.55 s (reduced heating rate from 620 °C), and the post tempering cooling rate was 60 °C/s. During the tempering cycle, a jaw distance of 9.5 mm was applied to ensure maximum heating and cooling rates. The detailed experimental conditions are listed in Table 2, and they provided a wide range of microstructures and mechanical properties within a 10.5 mm wide uniform heat affected zone for further testing and evaluation of SSFW parameters. The tempering temperature was selected based on previous results obtained from SSFW and TCS simulations on L80 [10]. In that work, a holding time of 1 s at 680 °C proved to be sufficient to temper the hard microstructures that form in this steel. For simplicity, the experimental heat cycles will in the following text and throughout the paper be defined by referring only to the peak temperature and the controlled cooling rate below 920 °C. For instance, the phrase “cooled from peak temperature 1300 °C at a rate of 5 °C/s” means that the specimen was first cooled at a rate of 60 °C/s from 1300 °C down to 920 °C and then at a rate of 5 °C/s further down to room temperature. An individual specimen will either be identified by its specimen ID given in Table 2 (e.g. A3) or, when it is more convenient, by a notation including the peak temperature followed by the cooling rate below 920 °C in brackets, e.g. “specimen 1300(5)”.

Dilatometer curves were plotted and analysed to identify the phase transformations. The specimens were marked with a permanent marker at the position of the thermocouple at the specimen surface. The marker was used to machine a V-notch exactly at the location of the peak temperature during the simulation. For each

**Table 2** Experimental heating cycles performed in the Smitweld TCS machine. The cooling rates refer to controlled cooling below 920 °C. From the peak temperature and down to 920 °C, the specimens were cooled at the highest obtainable rate (60 °C/s)

Specimen ID	Peak temperature [°C]	Cooling rate [°C/s]	Specimen ID	Peak temperature [°C]	Cooling rate [°C/s]	Tempering
A1	1300	1	B1	1300	1	680°C for 1 s
A2	1300	3	B2	1300	3	
A3	1300	5	B3	1300	5	
A4	1300	10	B4	1300	10	
A5	1300	60	B5	1300	60	
A6	1150	1	B6	1150	1	
A7	1150	3	B7	1150	3	
A8	1150	5	B8	1150	5	
A9	1150	10	B9	1150	10	
A10	1150	60	B10	1150	60	
A11	950	1	B11	950	1	
A12	950	3	B12	950	3	
A13	950	5	B13	950	5	
A14	950	10	B14	950	10	
A15	950	60	B15	950	60	

thermal cycle, three specimens were subjected to Charpy-V impact testing at 0 °C, as required by API 5CT (oil well applications) [11]. Half-size impact test specimens were machined with dimensions 55×10×5 mm<sup>3</sup>, as per the ASTM E23 standard [12], with the middle of the heat affected zone located at the middle of the specimen length. The 10-mm-long V-notch was machined with a root radius of 0.25 mm. The observed toughness values were divided by 0.55 to get full size Charpy toughness values [12]. The impact testing was performed by using a Zwick Charpy-V pendulum impact tester RKD 450D. Hardness measurements were done in the middle of the weld simulated region (peak temperature) using a Vickers hardness testing machine with 10 kg weight. A total of 5 measurements were taken in each simulated region. The specimens were mechanically polished and etched with 2% Nital solution for optical microscopy observations. Microstructural studies were executed in a Leica MEF4M light microscope with a Jenoptik ProgRes C10 plus digital camera by using normal bright field illumination. Image Access Easy Lab software was used to capture the pictures digitally. Fracture surface analysis was carried out using a ZEISS Ultra SEM. Fracture modes and percentage of shear fracture were determined. The SEM was operated at an acceleration voltage of 20 kV.

## 3 Results

### 3.1 Microstructures

Microstructures of the samples heated to a peak temperature of 1300 °C and cooled at different cooling rates are given in Fig. 3. The slowest cooling rate of 1 °C/s had resulted in the

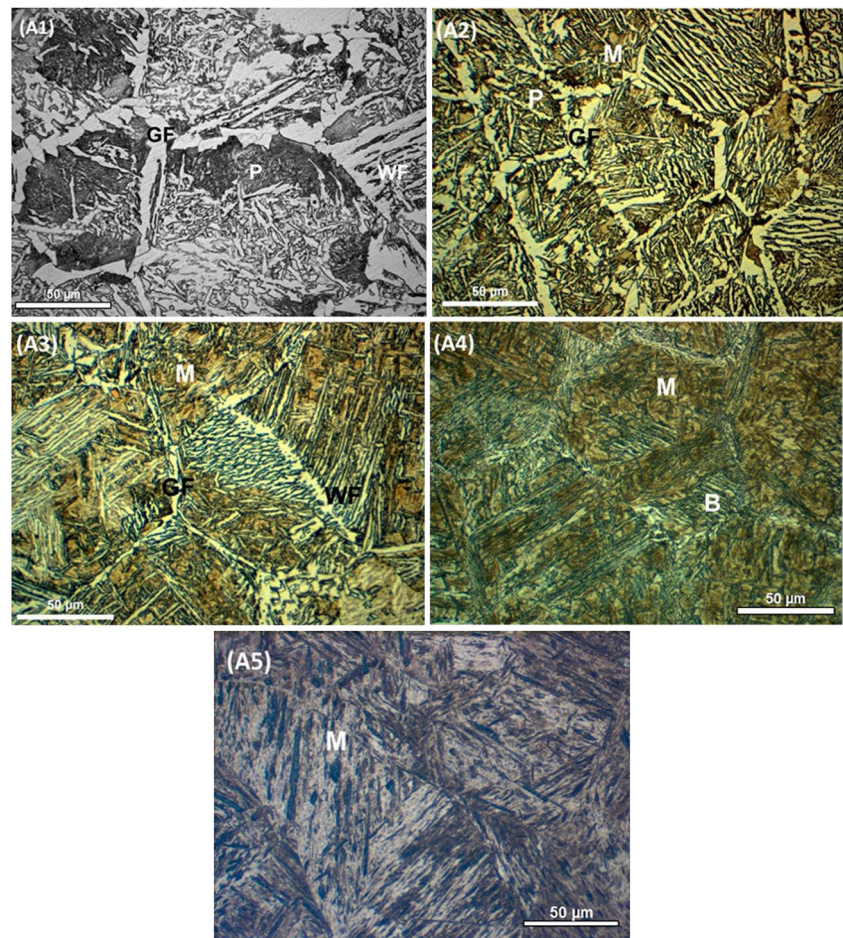
transformation of austenite to ferrite (F) and pearlite (P) (Fig. 3 A1). Two types of ferrite had formed, i.e. grain boundary ferrite (GF) at previous austenite grain boundaries (PAGB) and Widmanstätten ferrite (WF) within the previous austenite grains, where also the pearlite was located. Large pearlite colonies were occasionally located close to the grain boundary ferrite, but mostly the microstructure consisted of a fine mixture of pearlite and Widmanstätten ferrite plates/needles.

The microstructure for a cooling rate of 3 °C/s is presented in Fig. 3A2. A mixture of ferrite, pearlite (P), and martensite (M) was obtained for this cooling condition. Grain boundary ferrite (GF) is observed at PAGBs. A large fraction of Widmanstätten ferrite (WF) is also present mixed up with a coarse pearlite structure. In addition, a small fraction of martensite phase is present.

The microstructure of the 5 °C/s specimen is presented in Fig. 3A3. A mixed microstructure of grain boundary ferrite, Widmanstätten ferrite, and martensite can be observed. The martensite fraction has increased from the one formed at the lower cooling rate 3 °C/s (Fig. 3A2).

The microstructure of the 10 °C/s specimen is presented in Fig. 3A4. This relatively high cooling rate produced a mixture of martensite and bainite (B). Bainite was located both at previous austenite grain boundaries and within the previous austenite grains, while martensite had mainly formed within the austenite grains. The observed martensite fraction was higher than in the specimen cooled at 5 °C/s. The microstructure of the 60 °C/s specimen is presented in Fig. 3A5. A martensitic microstructure with a small fraction of bainite was observed in this specimen.

**Fig. 3** Microstructures of specimens cooled from 1300 °C, (A1) 1 °C/s, (A2) 3 °C/s, (A3) 5 °C/s, (A4) 10 °C/s, (A5) 60 °C/s



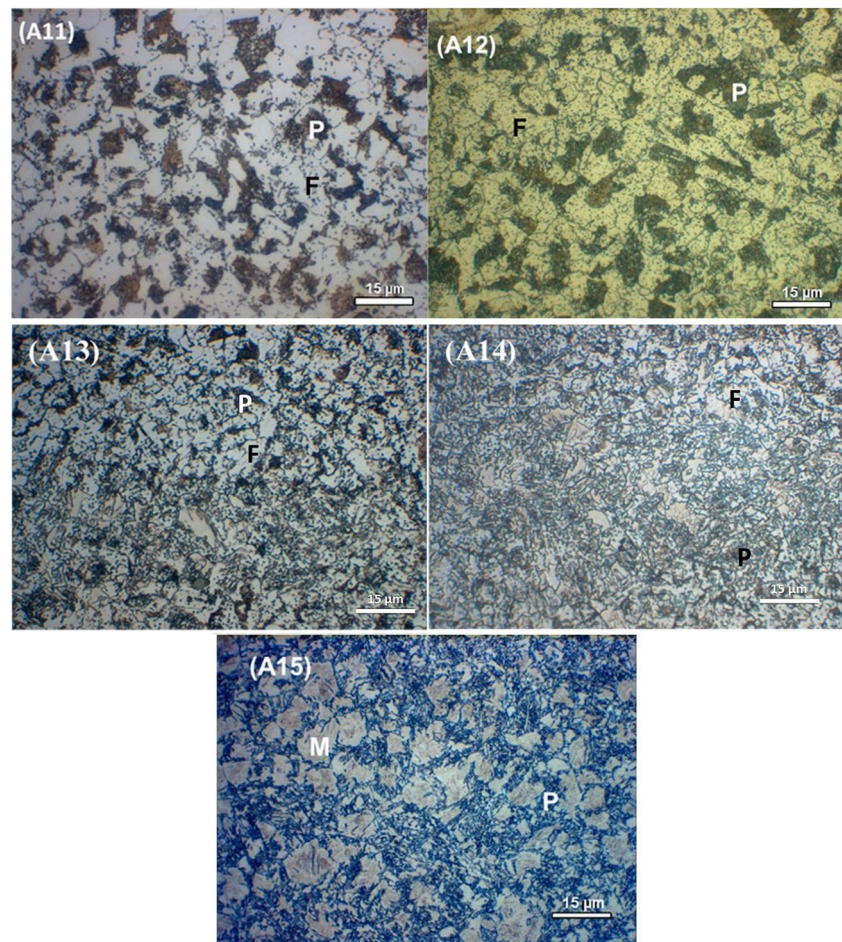
The microstructures of the specimens heated to 1150 °C were similar to the microstructures presented in Fig. 3 for specimens A1–A5. The peak temperature 1150 °C gave a smaller prior austenite grain size resulting in more refined microstructures, but otherwise, there were no significant differences in the microstructures in the two cases.

Microstructures of the specimens heat treated to a peak temperature of 950 °C are presented in Fig. 4A11–A15. All these specimens contained ferrite, and for the three lowest cooling rates, a well-defined mixture of more or less polygonal ferrite and pearlite had formed. The polygonal ferrite grain size decreased with increasing cooling rate, being typically 8 μm (A11) and 3–6 μm (A12 and A13). The polygonal grains were mixed up with a number of irregularly shaped ferrite grains, the smallest of those grains were probably sub-grains. The size of the pearlite colonies decreased with increasing cooling rate. In specimen A13, 2–3 μm large martensite islands were occasionally observed in addition to the ferrite and pearlite. In the specimen cooled at 10 °C/s (A14), the ferrite microstructure appeared rather chaotic, with a grain size varying between 0.5 (sub-grains) and 5 μm. Especially, the smallest grains were

very irregular in shape, some were needle-shaped, and the microstructure resembled that of acicular ferrite. Small colonies of pearlite (dark grey in Fig. 4A14) were mixed up with the ferrite, and as in specimen A13, martensite islands, up to 6 μm in size, were present. The microstructure of specimen A15, cooled at the highest cooling rate from 950 °C, was even more complex and consisted of about 40 volume-% martensite islands, up to 15 μm in size, surrounded by a complex mixture of sub-micron globular and needle-shaped ferrite (sub-)grains.

It might also be mentioned that, within the ferrite grains in specimens A11–A14, a number of sub-micron particles, probably carbides, were present (easily discernible in Fig. 4A12). Occasional and possible carbides (mostly sub-micron, but in rare cases up to 2 μm in size) were also observed in some of the other microstructures, e.g. close to Widmanstätten ferrite in Fig. 3A3. However, in all those cases, the size and distribution of these particles were not of a character that should have a decisive influence on the properties of the heat affected zone, and no evident effect of them could be discerned during the mechanical testing (Section 3.3). They are therefore not mentioned in the further text.

**Fig. 4** Microstructures of specimens cooled from 950 °C, (A11) 1 °C/s, (A12) 3 °C/s, (A13) 5 °C/s, (A14) 10 °C/s, (A15) 60 °C/s



### 3.2 Phase transformation behaviour

The changes in the specimen thickness dimension during heating and cooling were measured and recorded by a dilatometer. As an example of how phase transformation temperatures were extracted from these measurements, Fig. 5 shows the dilatometer curves recorded for specimen 1300(1) (specimen A1) and 1300(60) (specimen A5) during heating and cooling (8 s heating time to peak temperature, i.e. an average heating rate of 160 °C/s). It clearly shows the Ac1 temperature during heating and the phase transformations during cooling. The phase transformation start temperature is identified by the deviation from linearity in the cooling part of the curve. Table 3 gives the temperatures at which the transformation of the austenite started,  $T_s$ , and ended,  $T_f$ , in all specimens cooled from 1300 °C. (Note that only the  $T_s$  temperature of the phase that nucleated first is given in the table.) The highest  $T_s$  temperatures, 690–600 °C, indicates the start of transformation to ferritic microstructures (GBF, WF, P, B), while the lowest temperature 370 °C indicates the start of martensite formation (in the specimen cooled at 60 °C/s). The fraction of bainite in the latter specimen was too low to give a plateau in the dilatometer curve. Ferritic transformation was observed

at the lowest cooling rates 1–5 °C/s for all peak temperatures. For specimens that produced sufficient amounts of ferritic constituents in addition to martensite, two plateaus were present on the dilatometer curves. The martensite transformation start temperature was measured to be between 350 and 390 °C.

### 3.3 Hardness and toughness properties

The minimum specified tensile strength and maximum hardness of the L80 steel (base material) are according to API 5CT [11] 655 MPa and 254 HV, respectively. The minimum weld hardness to match the base material tensile strength would be 204 HV according to Ref. [13] which gives equivalent hardness and tensile strength values. Hardness values between 254 and 204 HV are thus required within the heat affected zone (HAZ) of welded L80 steel. In addition, a minimum HAZ toughness value of 27 J at 0 °C is required according to API 5CT [11].

The dependence of hardness on peak temperature and cooling rate is given in Table 4 and Fig. 6. On the whole, the hardness increased with increasing peak temperature and cooling rate, although a few individual values deviated from

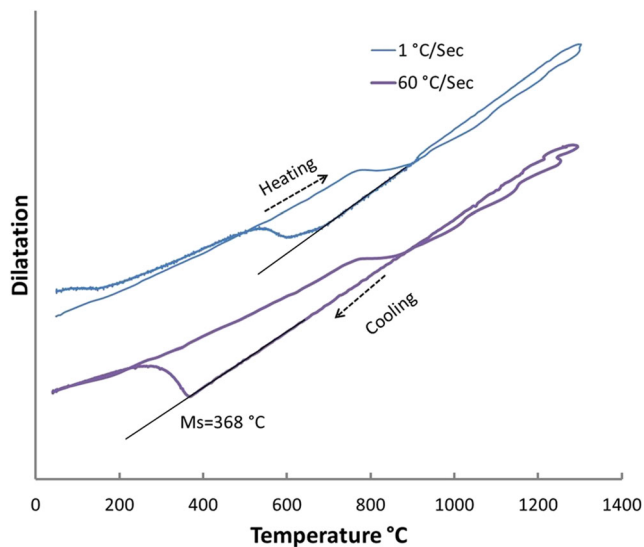


**Fig. 5** Dilatometer curves of specimens A1 and A5, heated to 1300 °C and cooled at 60 °C/s down to 920 °C and at 1 °C/s and 60 °C/s, respectively, from 920 °C (The dilatation axis has no scale since the graphs are vertically displaced relative to each other so that they easily can be separated.)

this general trend. For the highest cooling rate, the weld simulated hardness was much higher for the two highest peak temperatures than for the peak temperature 950 °C, which would be expected from the amounts of martensite formed in the specimens. As expected, the slowest cooling rate 1 °C/s produced for all peak temperatures the softest microstructure, ferrite (F/GF/WF), and pearlite.

Only the specimen cooled at a rate of 1 °C/s from peak temperature 950 °C had a hardness value below the minimum required hardness value of 204 HV. For peak temperature 1300 °C, cooling rates higher than 3 °C/s produced hardness values higher than the maximum limit 254 HV. The specimens cooled from 1150 °C at rates of 1 °C/s and 3 °C/s had hardness levels within acceptable limits.

Table 4 and Fig. 7 give hardness values measured after the tempering cycle. Tempering was carried out at 680 °C with 1-s holding time. On the whole, the hardness was reduced after

**Table 3** Transformation start and finish temperatures during cooling of specimens heated to 1300 °C at 160 °C/s and cooled at 60 °C/s down to 920 °C and at different rates below 920 °C

Cooling rate from 920 °C [°C/s]	Transformation start temperature $T_s$ [°C]	Transformation finish temperature $T_f$ [°C]
1	690	485
3	650	420
5	610	300
10	600	250
60	370	250

the tempering. However, the tempering gave only a small hardness reduction for most of the specimens that had been heated to a peak temperature of 950 °C due to the low contents or absence of martensite in these specimens. An exception was the  $T_p=950$  °C specimen that had been cooled at 60 °C/s and which contained a fair amount of martensite. In fact, the tempering effect increased with the amount of martensite present in the specimens. Nevertheless, the tempering effect on the specimens heated to 1150 °C and 1300 °C and cooled at 60 °C/s was not strong enough to reduce their hardness to an acceptable level. After tempering, all specimens except 950(1), 1150(10), 1150(60), and 1300(60) satisfied the API hardness requirements.

Impact full size toughness values as a function of cooling rate for the three different peak temperatures are given in Table 4 and in Fig. 8 for the untempered A-specimens and in Fig. 9 for the tempered B-specimens. The required minimum toughness value 27 J is given by the horizontal lines in Fig. 8 and Fig. 9.

For all peak temperatures, the untempered weld simulated toughness decreased with increasing cooling rate up to 10 °C/s, and for these low and medium cooling rates, the  $T_p=950$  °C specimens had toughness values that were well above those of the  $T_p=1150$  °C and  $T_p=1300$  °C specimens. For peak temperature 950 °C, the untempered toughness continued to drop with increasing cooling rate, while the untempered toughness of the specimens that had been heated to 1150 °C and 1300 °C increased when the cooling rate increased from 10 to 60 °C/s. All untempered  $T_p=950$  °C specimens except the ones that were cooled at 60 °C/s satisfied the API 5CT requirement of 27 J, while this was not the case for the  $T_p=1300$  °C specimens. Among the untempered  $T_p=1150$  °C specimens, only those cooled at the medium cooling rates 5 °C/s and 10 °C/s failed to meet the toughness requirement.

All specimens showed increased toughness after the tempering treatment, so all tempered specimens satisfied the acceptance criterion (see Fig. 9). For all cooling rates, the tempered specimens originally cooled from 950 °C had a higher toughness than the tempered specimens originally cooled from the other two peak temperatures. For all three peak temperatures, the tempering introduced a large increase in toughness for the specimens that were cooled at a rate of 10 °C/s or higher. For example, for the specimens that had been cooled at 60 °C/s from 950 °C, the toughness value increased by a factor of 10 upon tempering, from 18 to 180 J.

Figure 10 shows fracture surfaces of specimens 1300(1) and 1300(60). Cleavage facets are observed in specimen that had been cooled at a cooling rate of 1 °C/s. The fracture surface of specimen 1300(60) had a dimpled appearance, which indicates ductile fracture.

**Table 4** Hardness and toughness as a function of peak temperature and cooling rate, untempered and tempered (1 s at 680 °C) condition. Cooling rate refers to cooling rate below 920 °C

T <sub>P</sub> [°C]	Cooling rate [°C/s]	Hardness [HV10]	Toughness [J]	Tempered hardness [HV10]	Tempered toughness [J]
1300	1	223	27	213	30
1300	3	253	16	228	42
1300	5	270	14	237	54
1300	10	370	8	274	84
1300	60	483	73	288	109
1150	1	202	67	222	65
1150	3	233	34	219	54
1150	5	261	25	230	67
1150	10	324	14	256	103
1150	60	503	80	303	134
950	1	197	164	195	158
950	3	233	147	204	167
950	5	215	89	207	154
950	10	217	77	208	156
950	60	309	18	250	181

## 4 Discussion

### 4.1 Hardness and toughness as a function of peak temperature and cooling rate

The peak temperature and the cooling rate from the fully austenitic state determine the final microstructure, which in turn determines the mechanical properties of the material. Especially for carbon steels, the selection of cooling rate is vital for achieving a desired microstructure. Coarse austenite grains formed during heating to 1300 °C and 1150 °C peak temperatures, resulting in coarse microstructures after cooling. Figure 5 presents dilatometer curves for two different cooling rates from 1300 °C, indicating two different phase formation

sequences. There is a clear indication of a martensite transformation at temperatures between 390 and 350 °C for specimen 1300(60). For specimen 1300(1), the phase transformation to Widmanstätten ferrite and pearlite occurred in the temperature range ~670–550 °C. On the other hand, the corresponding dilatometer curve for specimen 950(1) (not shown) indicated growth of polygonal ferrite/pearlite at higher transformation temperatures, resulting in a hardness value of 197 HV that is below what is required.

The range of microstructures present in the middle of the untempered heat affected zone is reflected in the hardness plots in Fig. 6. For all three peak temperatures, the hardness of the final microstructure more or less increased with increasing cooling rate due to the formation of bainite and martensite

**Fig. 6** Hardness as a function of peak temperature and cooling rate, untempered condition

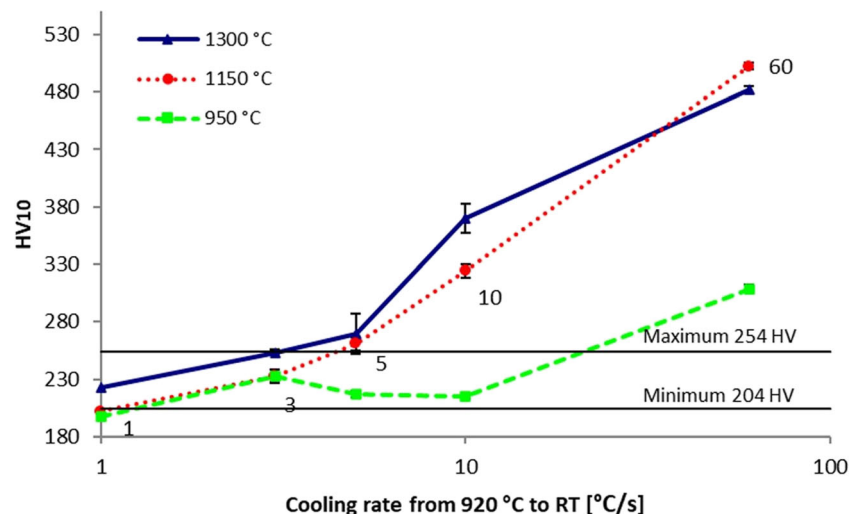
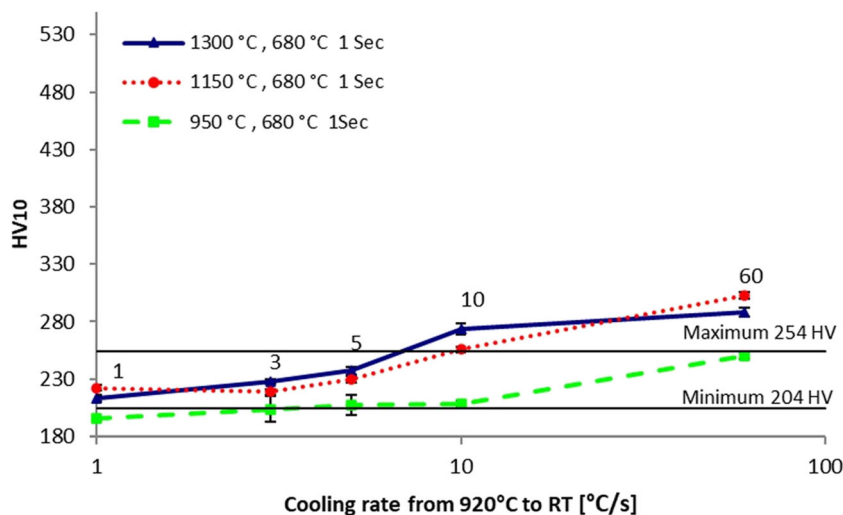




**Fig. 7** Hardness as a function of peak temperature and cooling rate after tempering for 1 s at 680 °C



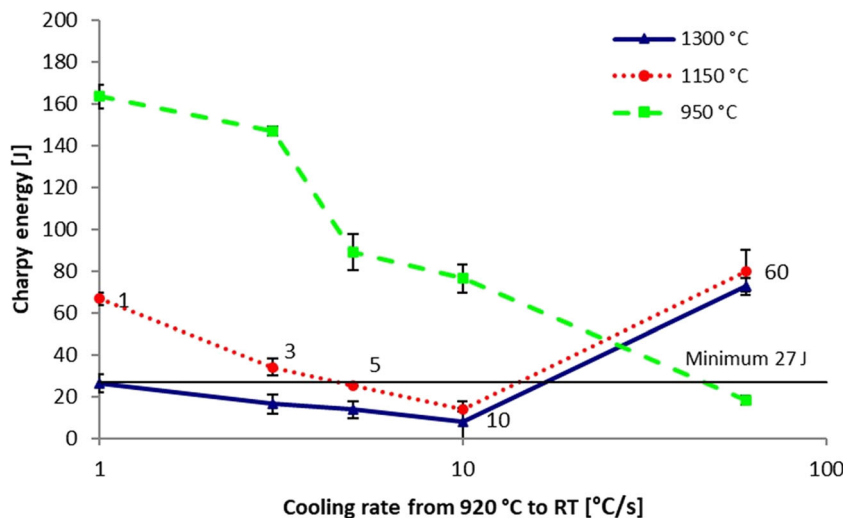
(for  $T_p = 950\text{ °C}$ , some martensite formed at the highest cooling rate). The two highest peak temperatures  $1150\text{ °C}$  and  $1300\text{ °C}$  gave very similar hardness values, and for the three highest cooling rates, the hardness values obtained for these peak temperatures were higher than those obtained for a peak temperature of  $950\text{ °C}$ . This is due to the heavy austenite grain growth that generally occurs at high temperatures, leading to low temperature formation of hard and similar microstructures (bainite, martensite) during medium fast and rapid cooling. Due to a finer austenite grain size and formation of higher fractions of softer (more stable) phases, the hardness values obtained for  $T_p = 1150\text{ °C}$  are lower than those obtained for  $T_p = 1300\text{ °C}$ , except for the highest cooling rate  $60\text{ °C/s}$  that produced fully martensitic microstructures. A plausible reason for this exception is that the finer austenite of the  $1150\text{ °C}$  specimen produced a finer martensite during cooling, resulting in a higher hardness due to a larger boundary area. Annealing at  $950\text{ °C}$ , however, produced a fine-grained austenite that during cooling transformed to softer ferritic

microstructures mixed up with a high fraction of martensite during cooling at  $60\text{ °C/s}$ , resulting in a higher hardness for that cooling rate

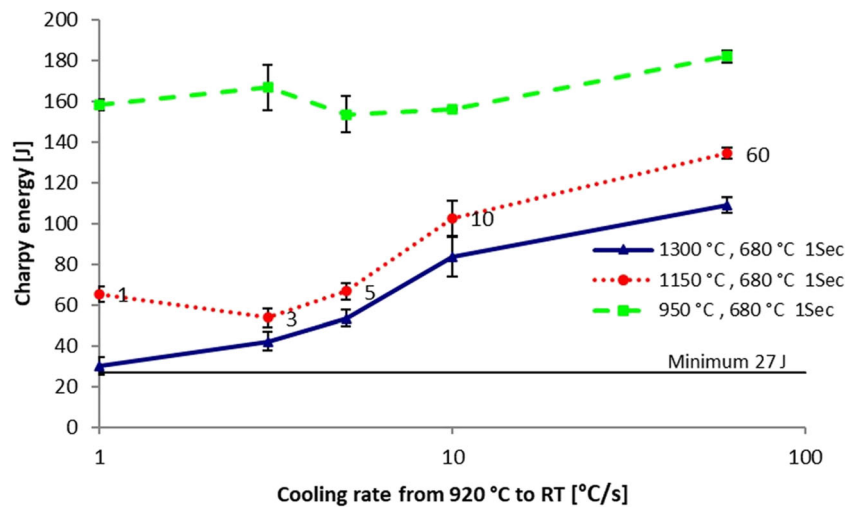
Tempering reduced the hardness of all specimens (Fig. 7), and the reduction was largest for the specimens that contained much martensite. However, the hardness reduction was not large enough to bring the samples that contained most martensite (specimens  $1300(60)$ ,  $1300(10)$ ,  $1150(60)$ ,  $1150(10)$ ,  $950(60)$ ) well below the maximum hardness limit of  $254\text{ HV}$ .

Figure 8 shows that, in most cases, the toughness of the untempered heat affected zone decreased with increasing cooling rate. The general reason for such a trend is the formation of more brittle microstructure constituents (WF, P, B, M) with increasing cooling rate. Exceptions from this general trend occurred for the highest cooling rate combined with the two highest peak temperatures, which resulted in the highest toughness values for these peak temperatures. The reason for this could be that almost exclusively martensite was formed at these two conditions, while the corresponding

**Fig. 8** Impact toughness at  $0\text{ °C}$  as a function of peak temperature and cooling rate, untempered condition



**Fig. 9** Impact toughness at 0 °C as a function of peak temperature and cooling rate after tempering for 1 s at 680 °C



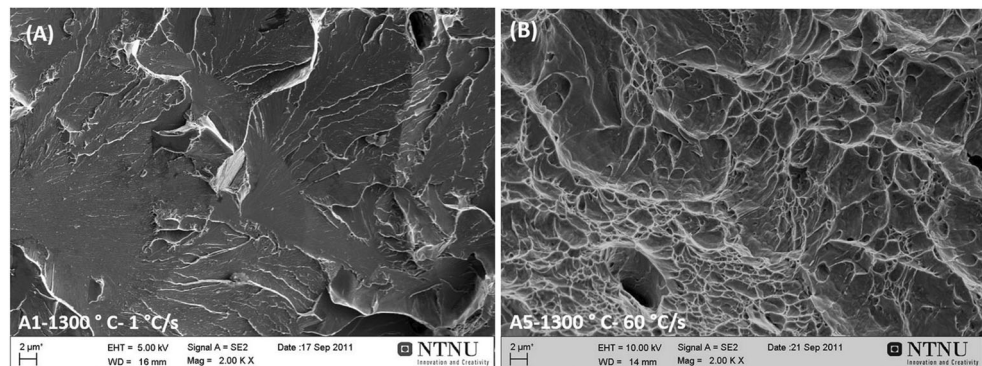
specimens cooled at lower cooling rates contained constituents like upper bainite and Widmanstätten ferrite. It seems that the latter constituents, containing aligned carbide particles or pearlite along lath/needle boundaries, in the present case are more brittle than plain martensite formed from austenite grain boundaries. In addition, some self-tempering may have occurred in the martensite below the  $M_s$  temperature 392 °C, giving a positive contribution to the toughness. This is known to take place in steels of much lower carbon contents, but they have, of course, a higher martensite transformation temperature. The fracture surface of the  $T_p = 1300$  °C specimen cooled at the lowest cooling rate contained cleavage facets, whereas the fracture surface of the corresponding specimen cooled at the highest cooling rate contained dimples (Fig. 10). This is a good illustration of the toughness difference between a martensitic specimen and a specimen containing coarse Widmanstätten ferrite and pearlite in the present steel. Satisfactory mechanical properties after isothermal transformation below the  $M_s$  temperature have been reported earlier (see e.g. Ref. [14]).

Since fine austenite grains result in fine-grained ferrite microstructures, the toughness of the specimens heated to 950 °C was in general higher than the toughness obtained for the two other peak temperatures, except for the highest cooling rate

°C/s which produced a brittle structure in the  $T_p = 950$  °C specimen. Possibly, the martensite is more brittle in this specimen than in the other specimens. Figure 4A15 shows that the microstructure of the  $T_p = 950$  °C specimen consists of martensite surrounded by a very fine-grained ferrite (probably sub grains) mixed up with some pearlite. During cooling of this specimen, the austenite transformation has obviously started by the nucleation of fine-grained polygonal ferrite on fine-grained austenite grain boundaries. As the ferrite grew into the austenite grains, carbon might have been pushed ahead of the growth front, enriching the austenite on carbon. At the upper transformation temperatures, this resulted in the nucleation of some pearlite. But as the temperature decreased, the pearlite growth probably stopped, and finally the carbon enriched austenite in the middle of the small austenite grains transformed to martensite that was more carbon rich and brittle than the martensite formed during cooling from higher peak temperatures, which produced much larger austenite grains (and longer diffusion distances).

Tempering at 680 °C increased the toughness of most specimens, especially of those which contained much martensite, and all tempered specimens satisfied the minimum toughness criterion. For the  $T_p = 950$  °C specimens, the tempering had a relatively strong effect on the toughness of the specimens that

**Fig. 10** Fracture surfaces of specimens cooled from 1300 °C peak temperature at rates of **a** 1 °C/s and **b** 60 °C/s



had been cooled at the three highest cooling rates and may be stronger than what would be predicted from the hardness reductions. Obviously, most of the toughness increase of the specimen cooled at 60 °C/s is due to tempering of a high fraction of martensite. In the specimens cooled at 5 °C/s and 10 °C/s; however, the martensite contents was probably too low to explain the toughness increase alone, although the 10 °C/s specimen contained some large martensite islands. But in addition to martensite, these specimens contained small pearlite colonies, probably formed at fairly low temperatures and probably containing thin carbide plates with sharp edges that could be detrimental to the toughness. The tempering at high temperature may have rounded off these sharp edges and by that increased the toughness of the steel (without affecting its hardness).

## 4.2 Selection of thermal cycles for SAG-FW

An important intent of this study is to acquire a set of data from TCS experiments that can give guidance on parameter selections for SAG forge welding of an L80 casing grade steel. For this purpose, it is necessary to do an evaluation of how plastic deformation will alter the graphs for the mechanical properties in Figs. 6, 7, 8, and 9. SAG-FW is a solid state welding process in which mating surfaces are heated by resistance or induction heating before being forged together. The plastic deformation introduced by forging during the SAG-FW process will cause a refinement of the austenite microstructure through either recrystallization or recovery, depending on the deformation temperature, resulting in a reduction in the austenite grain size and/or formation of sub grains within the austenite grains, both of which will in most cases favour transformation to finer and tougher microstructures at the expense of brittle coarse-grained microstructures containing large ferrite/pearlite grains/colonies, Widmanstätten ferrite, bainite, and/or martensite. The forging stage should therefore shift most of the toughness values in Figs. 8 and 9 upwards. Exceptions would occur if the softening reactions result in an austenite grain size of the same magnitude as that obtained in the present TCS specimens heated to 950 °C. If that happens, very rapid cooling may produce a brittle microstructure (Fig. 4A15) after cooling to room temperature.

In previous works on L80 casing grade steel, quenching of TCS specimens heated to 1150 °C resulted in a prior austenite grain size of 35 µm [10, 15], and forge welding at 1300 °C in a small-scale SAG-FW machine gave a prior austenite grain size of 45 µm [2]; i.e. the recrystallization following the plastic deformation nearly halved the austenite grain size obtained at 1300 °C in the present work (80 µm). Thus, for a welding temperature of 1300 °C, the forging stage reduces the austenite grain size to a value that is well above the austenite grain size of TCS specimens heated to 1150 °C. Most probably therefore, forging at peak temperature 1300 °C will increase

the toughness to values that are below the values given by the 1150 °C graphs in Figs. 8–9. Thermal cycles to a peak temperature of 1300 °C and cooling rates of 3, 5, and 10 °C/s are therefore still doubtful for forge welding of the L80 grade steel, unless a post weld heat treatment is carried out.

Also for a peak temperature of 1150 °C, forging will reduce the austenite grain size, but, of course, the true value is impossible to guess. If recrystallization nearly halves the grain size, as is the case for  $T_p = 1300$  °C, the value would be somewhere near 20 µm. It is not believed that the austenite grain size will become as low as 10–15 µm which from Fig. 4A11 is estimated to be the prior austenite grain size for  $T_p = 950$  °C during TCS. (Grain growth of recrystallized grains would probably prevent that.) If an austenite grain size based on these assumptions is assumed, the toughness graphs in Fig. 8 indicate that the cooling rates 1, 3, 5 °C/s, and may be 10 °C/s, probably will result in acceptable toughness after forge welding at 1150 °C. However, a cooling rate of 60 °C/s is questionable due to the risk of formation of brittle martensite *if* the prior austenite grain size becomes too low. If tempering is applied, all cooling rates for peak temperature 1150 °C should give acceptable toughness (cf. Fig. 9).

For the lowest peak temperature 950 °C, only TCS specimens cooled at 60 °C/s failed to meet the toughness criterion unless tempering was done. At this temperature, deformation induced recrystallization may not occur or may not be completed, especially for the highest cooling rates which reduce the time and temperature for recrystallization. However, also recovery and/or deformation structures within the deformed austenite will increase the nucleation of ferrite grains, and this may reduce the amount of brittle martensite that caused the low toughness of the TCS specimen A15 (cf. Fig. 4A15). However, whether a forging stage will increase the toughness of welds processed at 950 °C and cooled at 60 °C/s above the critical lower limit is still questionable, unless post weld tempering is performed (cf. Fig. 9).

How plastic deformation at the peak temperature will affect the hardness graphs is more difficult to foresee since austenite grain refinement will have both a positive and a negative effect on the final hardness. In Fig. 6, forging will possibly shift the graph for  $T_p = 1300$  °C towards the position of the 1150 °C graph in the diagram since similar microstructures were formed for those peak temperatures during the TCS simulations. Therefore, forge welding at 1300 °C combined with cooling rates 5, 10, and 60 °C/s will probably produce too hard welds. From Fig. 7 (and assuming that the forging step will cause the 1300 °C graph to approach the 1150 °C graph in the diagram), it is seen that a tempering of 1 s at 680 °C will not reduce the 1300 °C forge welded hardness to acceptable values for the cooling rates 10 and 60 °C/s, but that a cooling rate of 5 °C/s probably is a possible choice if tempering is carried out. In addition, for  $T_p = 1300$  °C, the cooling rates 1 and 3 °C/s should result in acceptable hardness values both

with and without post weld tempering. (However, tempering is required to fulfil the toughness requirement for 3 °C/s and 5 °C/s.)

Also for  $T_p = 1150$  °C, it is reasonable to believe that the forging step will cause the hardness graphs to be shifted downwards in the diagrams since a reduced austenite grain size in general will cause increased nucleation of more stable and soft phases. However, a refinement of the microstructure is also likely to give a positive hardness contribution. Bearing this in mind, the cooling rates 10 °C/s and, especially, 60 °C/s are likely to produce too hard forge welds (without post weld tempering). Both 3 °C/s and 5 °C/s are candidate cooling rates, assuming that forging increases the amount of soft grain boundary ferrite. For the lowest cooling rate 1 °C/s, only ferrite and pearlite formed for all peak temperatures during the TCS experiments. The hardness for the 1150(1) specimen was measured at 202 HV, very close to the minimum requirement. It is reasonable to believe that a forging step will increase this value because of microstructure refinement, but the situation is uncertain since, for the TCS specimens, the hardness of the ferrite-pearlite microstructures decreased with decreasing ferrite grain size (Fig. 6), probably because of decreasing amounts of pearlite with decreasing austenite grain size (closer to equilibrium). From Fig. 7, it is seen that, if a post weld temper of 1 s at 680 °C is performed, a cooling rate of 10 °C/s is also a possible cooling rate, assuming that forging reduces the hardness through reduced austenite grain size and increased amounts of (grain boundary) ferrite for this cooling rate.

For peak temperature 950 °C, ferrite-pearlite was formed at all cooling rates except at 60 °C which resulted in martensite islands within a very fine-grained ferrite matrix. For the cooling rates 1, 3, 5, and 10 °C/s, the forging step might increase the hardness through an increase in the nucleation sites for ferrite, but it is believed that this only occurs to a limited degree since the grain size even without the forging step is very/extremely small, and the driving force for grain growth is strong for small grains. Thus, it is believed that the weld hardness after forge welding at 950 °C will be well below the maximum limit. Moreover, forging will probably increase the hardness obtained for 1 °C/s above the minimum value 204 HV. Earlier in this section, it was suggested that forging might reduce the amount of brittle martensite that formed at the highest cooling rate from 950 °C during TCS. Whether this will reduce the hardness to an acceptable value is, however, uncertain, and tempering may be required for this cooling rate. Otherwise, tempering is probably unnecessary after forge welding at 950 °C and should be avoided due to the risk of reducing the hardness below the lower limit (see Fig. 7).

In summary, taking both toughness and hardness requirements into consideration, the most reliable thermal parameters for forge welding are as follows:

- Forging at 1300 °C followed by cooling at 1 °C/s without subsequent tempering, or cooling at 1, 3, or 5 °C/s if welding is followed by tempering (1 s at 680 °C).
- Forging at 1150 °C followed by cooling at 1, 3, or 5 °C/s without or with subsequent tempering (cooling rate 10 °C/s may also be a possibility).
- Forging at 950 °C followed by cooling at 1, 3, 5 or 10 °C/s without subsequent tempering or cooling at 60 °C/s if welding is followed by tempering).

Of course, steel geometry and dimensions will have an effect on local temperature gradients and cooling conditions and must be taken into consideration to avoid spots of too low strength or toughness.

## 5 Conclusions

Weld thermal simulation of an API 5CT L80 steel (with and without subsequent tempering) has been performed and analysed. Specimens were subjected to three different peak temperatures (1300 °C, 1150 °C, 950 °C) and five different cooling rates (1 °C/s, 3 °C/s, 5 °C/s, 10 °C/s, 60 °C/s) below 920 °C after having been rapidly cooled to this temperature from the peak temperature. The resulting microstructures and mechanical properties have been studied. The following conclusions from the thermal simulation experiments are relevant for finding optimum peak temperatures and cooling conditions for welding of L80 components by the SAG-FW technique.

- For all peak temperatures, the highest cooling rate 60 °C/s produced varying fractions of martensite, and the lowest cooling rate 1 °C/s produced a mixture of pearlite and ferritic constituents like polygonal ferrite, grain boundary ferrite, and Widmanstätten ferrite. Intermediate cooling rates produced mixtures of ferrite, bainite, and martensite.
- For each peak temperature, the highest cooling rate(s) produced microstructures that failed to meet either the hardness (204 < HV < 254) or the toughness (> 27 J) acceptance criterion, or both. The higher the peak temperature was, the fewer cooling rates gave acceptable mechanical properties.
- Tempering at 680 °C for 1 s increased the toughness significantly, and to acceptable values for all cooling rates for all three peak temperatures. However, the four specimens cooled at the two highest cooling rates from the two highest peak temperatures did still not satisfy the *maximum hardness* requirement.
- A peak temperature of 950 °C followed by cooling at 1 °C/s gave a very high toughness, even without tempering, but this treatment resulted in a hardness that was less than the minimum hardness requirement for the alloy. Subsequent tempering reduced the hardness to even a lower value.

- Based on the results from the thermal weld simulations and a discussion of how a forging stage will affect the mechanical properties of a real forge weld, the following combinations of peak temperature in °C and cooling rate in °C/s (in brackets) are promising parameters for welding L80 steel components by the SAG-FW technique, without post weld heat treatment: 1300(1); 1150(1,3,5); and 950(1,3,5,10).
- The following combinations of peak temperature and cooling rate are promising parameters for welding L80 steel components by the SAG-FW technique followed by post weld heat treatment at 680 °C for 1 s: 1300(1,3,5); 1150(1,3,5); and 950(60).

**Acknowledgements** The authors are thankful to the Faculty of Natural Sciences, Norwegian University of Science and Technology, AMR Engineering AS, and Tube Fuse Technology Ltd for financing the project and for giving technical support. Sincere thanks are also due to Eng. Pål Ulseth, Department of Materials Science and Technology, NTNU, for his assistance during sample preparation and to Senior Adviser Hans Iver Lange, Materials and Nanotechnology, Sintef Industry, Trondheim, Norway, for his assistance during the toughness testing.

**Author contribution** All authors contributed to the study conception and design. Material preparation, experimental work, and data collection were performed by Vinothkumar Palanisamy. Analysis of the results was performed by all authors. The work was supervised by Jan Ketil Solberg, Bjarne Salberg, and Per Thomas Moe. The first draft of the manuscript was written by Vinothkumar Palanisamy. Jan Ketil Solberg and Per Thomas Moe commented and wrote supplements to the first version. The final manuscript was read and approved by Vinothkumar Palanisamy, Jan Ketil Solberg, and Per Thomas Moe.

**Funding** Open access funding provided by NTNU Norwegian University of Science and Technology (incl St. Olavs Hospital - Trondheim University Hospital). The researched work was carried out within a PhD project financed by the Faculty of Natural Sciences, Norwegian University of Science and Technology, Trondheim, Norway. Some experimental work was in addition financed by AMR Engineering AS, Drammen, Norway, and by Tube Fuse Technology Ltd, UK.

**Data availability** The authors guarantee that this manuscript is an honest, accurate, and transparent report of the research work that has been executed. No important aspects of the work have been omitted.

**Code availability** Not applicable.

## Declarations

**Conflict of interest** The authors declare no competing interests.

**Open Access** This article is licensed under a Creative Commons Attribution 4.0 International License, which permits use, sharing, adaptation, distribution and reproduction in any medium or format, as long as you give appropriate credit to the original author(s) and the source, provide a link to the Creative Commons licence, and indicate if changes were made. The images or other third party material in this article are included in the article's Creative Commons licence, unless indicated otherwise in a credit line to the material. If material is not included in the article's

Creative Commons licence and your intended use is not permitted by statutory regulation or exceeds the permitted use, you will need to obtain permission directly from the copyright holder. To view a copy of this licence, visit <http://creativecommons.org/licenses/by/4.0/>.

## References

1. GS Marimuthu, PhD Thesis: Small Scale Forge Welding, Process design and analysis, 2013, Department of Engineering Design and Materials, Norwegian University of Science and Technology (NTNU), Trondheim.
2. Vinothkumar P, Ganesan SM, Solberg JK, Salberg B, Moe PT (2012) Studies on shielded active gas forge welded API 5CT L80 material at different cooling rates. *Adv Mater Res* 409:871–876
3. Boumerzoug Z, Raouche E, Delaunois F (2011) Thermal cycle simulation of welding process in low carbon steel. *Mater Sci Eng A* 530:191–195
4. Dunder M, Samardžić I, Klarič S (2007) Influence of cooling time  $\Delta t_{8/5}$  on welded joint properties of the thermal cycle simulated TStE 420 specimens. *Tehnički Vjesnik* 14(1,2):47–57
5. Shi Y, Han Z (2008) Effect of weld thermal cycle on microstructure and fracture toughness of simulated heat-affected zone for a 800 MPa grade high strength low alloy steel. *J Mater Process Technol* 207:30–39
6. Moeinifar S, Kokabi AH, Hosseini HRM (2010) Influence of peak temperature during simulation and real thermal cycles on microstructure and fracture properties of the reheated zones. *Mater Des* 31:2948–2955
7. Zheng S, Wu Q, Huang Q, Liu S, Han Y (2011) Influence of different cooling rates on the microstructure of the HAZ and welding CCT diagram of CLAM steel. *Fusion Eng Des* 86:2616–2619
8. Andrew KW (1965) Empirical formulae for the calculation of some transformation temperatures. *JISI* 203:721–727
9. W Steven and AG Haynes (1956) The Temperature of Formation of Martensite and Bainite in Low Alloy Steels. *JISI* 183: 349–359
10. Ø. A. Ellingsen, MSc thesis: Forge welding of the non-weldable steel qualities K55, L80 and L80SS, Department of Materials Science and Engineering, Norwegian University of Science and Technology (NTNU), Trondheim, 2010.
11. *Casing and Tubing, API Specifications 5CT*, 10th ed.; 2018. Available online: <https://www.api.org/products-and-services/standards/important-standards-announcements/standard-5ct> (accessed on 27.01.2021).
12. ASTM E23, Standard test methods for notched bar impact testing of metallic materials, 2002.
13. BBS Stål & Metall, Hardness conversion table—tensile strength, Vickers, Brinell och Rockwell (according to DIN 50150). Available online: <https://www.bbshalmstad.se/en/infocenter/hardness-conversion-table> (accessed on 27.01.2021).
14. da Cruz JA jr, Santos DB (2013) Effect of tempering temperature on isothermal decomposition product formed below Ms. *J Mater Res Technol* (2):93
15. V. Palanisamy, B. Salberg, J. K. Solberg, and P. T. Moe, Microstructure and Mechanical properties of API 5CT L80 casing grade steel quenched from different temperatures, OMAE2012-83937, 31th International Conference on Ocean, Offshore and Arctic Engineering, June 10–12, 2012, Rio Di Janeiro.

**Publisher's note** Springer Nature remains neutral with regard to jurisdictional claims in published maps and institutional affiliations.